REFERENCES AND NOTES

1. S. Picozzi, C. Ederer, *J. Phys. Condens. Matter* **21**, 303201 (2009).
2. T. Kimura, *Annu. Rev. Condens. Matter Phys.* **3**, 93–110 (2012).
3. X. Rocquefelte, K. Schwarz, P. Blaha, S. Kumar, J. van den Brink, *Nat. Commun.* **4**, 2511 (2013).
4. K. Noda, M. Akaki, T. Kikuchi, D. Akahoshi, H. Kuwahara, *J. Appl. Phys.* **99**, 08S905 (2006).
5. N. Abe *et al.*, *Phys. Rev. Lett.* **99**, 227206 (2007).
6. H. Murakawa *et al.*, *Phys. Rev. Lett.* **101**, 197207 (2008).
7. F. Kagawa *et al.*, *Phys. Rev. Lett.* **102**, 057604 (2009).
8. E. Schierle *et al.*, *Phys. Rev. Lett.* **105**, 167207 (2010).
9. N. Abe, K. Taniguchi, H. Sagayama, H. Umetsu, T. Arima, *Phys. Rev. B* **83**, 060403(R) (2011).
10. F. Kagawa, Y. Onose, Y. Kaneko, Y. Tokura, *Phys. Rev. B* **83**, 054413 (2011).
11. I. Fina, L. Fàbrega, X. Martí, F. Sánchez, J. Fontcuberta, *Phys. Rev. Lett.* **107**, 257601 (2011).
12. D. Meier *et al.*, *Phys. Rev. Lett.* **102**, 107202 (2009).
13. T. Hoffmann, P. Thielen, P. Becker, L. Bohatý, M. Fiebig, *Phys. Rev. B* **84**, 184404 (2011).
14. T. Kimura *et al.*, *Nature* **426**, 55–58 (2003).
15. M. Kenzelmann *et al.*, *Phys. Rev. Lett.* **95**, 087206 (2005).
16. B. Lorenz, *ISRN Condens. Matter Phys.* **2013**, 497073 (2013).
17. H. Katsura, N. Nagaosa, A. V. Balatsky, *Phys. Rev. Lett.* **95**, 057205 (2005).
18. M. Mostovoy, *Phys. Rev. Lett.* **96**, 067601 (2006).
19. H. C. Walker *et al.*, *Phys. Rev. B* **88**, 214415 (2013).
20. D. Meier, N. Aliouane, D. N. Argyriou, J. A. Mydosh, T. Lorenz, *New J. Phys.* **9**, 100 (2007).
21. D. Senff, P. Link, N. Aliouane, D. N. Argyriou, M. Braden, *Phys. Rev. B* **77**, 174419 (2008).
22. M. Fiebig, V. V. Pavlov, R. V. Pisarev, *J. Opt. Soc. Am. B* **22**, 96–118 (2005).
23. S. A. Denev, T. T. A. Lummen, E. Barnes, A. Kumar, V. Gopalan, *J. Am. Ceram. Soc.* **94**, 2699–2727 (2011).
24. See the supplementary materials on *Science* Online.
25. A. K. Tagantsev, L. Eric Cross, J. Fousek, *Domains in Ferroic Crystals and Thin Films* (Springer, New York, 2010).
26. N. Aliouane *et al.*, *Phys. Rev. Lett.* **102**, 207205 (2009).
27. N. Abe, K. Taniguchi, S. Ohtani, H. Umetsu, T. Arima, *Phys. Rev. B* **80**, 020402(R) (2009).
28. A. N. Kolmogorov, *Bull. Acad. Sci. USSR Phys. Ser.* **1**, 355–359 (1937).
29. P. Tolédano, *Phys. Rev. B* **79**, 094416 (2009).
30. M. Mochizuki, N. Furukawa, *Phys. Rev. Lett.* **105**, 187601 (2010).
31. M. Mochizuki, N. Furukawa, N. Nagaosa, *Phys. Rev. B* **84**, 144409 (2011).
32. T. Kimura, Y. Sekio, H. Nakamura, T. Siegrist, A. P. Ramirez, *Nat. Mater.* **7**, 291–294 (2008).
33. T. Aoyama *et al.*, *Nat. Commun.* **5**, 4927 (2014).
34. M. Mochizuki, N. Nagaosa, *Phys. Rev. Lett.* **105**, 147202 (2010).
35. T. Kubacka *et al.*, *Science* **343**, 1333–1336 (2014).

ACKNOWLEDGMENTS

We thank M. Trassin and T. Arima for fruitful discussions. This work was supported by the Swiss National Science Foundation (SNSF) (grant nos. 200021_147080/1 and 200021_144115), the NCCR Molecular Ultrafast Science and Technology (NCCR MUST) research instrument of the SNSF, and Grants-in-Aid for Scientific Research, Japan Society for the Promotion of Science (JSPS KAKENHI) (grant nos. 24244058, 25870169, and 25287088), MEXT, Japan. M.Mo. was supported by JSPS KAKENHI (grant nos. 25870169 and 25287088).

SUPPLEMENTARY MATERIALS

www.sciencemag.org/content/348/6239/1112/suppl/DC1
Materials and Methods
Supplementary Text
Figs. S1 to S4
References (*36*–*38*)

28 August 2014; accepted 5 May 2015
10.1126/science.1260561

FRICTION

Tuning friction atom-by-atom in an ion-crystal simulator

Alexei Bylinskii,* Dorian Gangloff,* Vladan Vuletić†

Friction between ordered, atomically smooth surfaces at the nanoscale (nanofriction) is often governed by stick-slip processes. To test long-standing atomistic models of such processes, we implemented a synthetic nanofriction interface between a laser-cooled Coulomb crystal of individually addressable ions as the moving object and a periodic light-field potential as the substrate. We show that stick-slip friction can be tuned from maximal to nearly frictionless via arrangement of the ions relative to the substrate. By varying the ion number, we also show that this strong dependence of friction on the structural mismatch, as predicted by many-particle models, already emerges at the level of two or three atoms. This model system enables a microscopic and systematic investigation of friction, potentially even into the quantum many-body regime.

Stick-slip friction is a nonlinear phenomenon in which two surfaces stick to each other owing to a static friction force and accumulate potential energy under increasing applied shear force, then slip suddenly. As the released energy is dissipated, the surfaces stick again, and the process repeats (*1*). This phenomenon occurs on length scales ranging from nanometers [biological molecules and atomic contacts (*1*–*3*)] to the kilometer scales of earthquakes (*4*). Interestingly, at the nanoscale, lattice mismatch between surfaces can cancel the sticking forces, resulting in continuous and almost frictionless sliding termed superlubricity (*5*). Despite their fundamental and technological importance, stick-slip and superlubricity are not fully understood because of the difficulty of probing an interface with microscopic resolution and control.

The simplest atomistic friction model is the single-particle stick-slip model by Prandtl and Tomlinson (PT) (*6*, *7*). The particle, held in a harmonic potential of an elastic object crystal, is driven across a sinusoidal potential of a rigid substrate crystal. This one-particle model, however, fails to capture the effects of structural mismatch between the crystal surfaces. The Frenkel-Kontorova (FK) model (*8*, *9*) instead treats the object as an infinite array of atoms joined by springs. This model is governed by the commensurability of the unperturbed array and the substrate and exhibits nontrivial kink dynamics (*8*), the pinned-to-sliding Aubry phase transition (*10*), and the related superlubricity (*5*).

Tools based on atomic force microscopy (*11*) can measure atomic-scale slips between surfaces comprising down to a few atoms (*12*–*14*). This has enabled the observation of superlubricity by varying the normal load (*15*) or the relative orientation of crystal lattices forming the interface (*16*, *17*). Most observations in these systems can be qualitatively explained via variants of the PT or FK models but without direct access to microscopic dynamics. Kink propagation dynamics, however, was observed in a macroscopic friction simulator with colloidal polystyrene beads in an optical lattice (*18*).

Here, following recent proposals (*19*–*22*), and enabled by the recent trapping of an ion in an optical lattice (*23*–*25*), we introduce an experimental system that allows us to study and control nanofriction at the individual-atom level. We form a nanofriction interface (Fig. 1A) by transporting a trapped-ion crystal with tunable spacings (*26*) over the sinusoidal potential of an optical standing wave (optical lattice), emulating an elastic crystal moving over a rigid periodic substrate. We measure the static friction force and the dissipated energy for each individual ion by tracking its position with sublattice spatial resolution and time resolution below the thermal relaxation time scale.

$^{174}Yb^{+}$ ions, laser cooled to sub-millikelvin temperatures, are held in a linear Paul trap with harmonic confinement (*27*), where they self-organize into an inhomogeneous one-dimensional crystal owing to their mutual Coulomb repulsion. Adding the sinusoidal optical-lattice potential (*23*, *28*) produces a corrugated external potential V for each ion, given by $V/(m\omega_0^2 a^2) = \frac{1}{2}\left(\frac{x_i - X}{a}\right)^2 + \eta \cdot \frac{1}{4\pi^2}\cos\left(\frac{2\pi}{a}x_i\right)$ (Fig. 1A). Here, m is the ion's mass, a = 185 nm is the optical-lattice period, x_i is the ion's position, and X is the center of the Paul trap. This potential is characterized by the dimensionless corrugation parameter η, equal to the confinement ratio $(\omega_L/\omega_0)^2$ of the lattice site vibrational frequency $\omega_L/(2\pi)$ to the Paul trap longitudinal vibrational frequency $\omega_0/(2\pi)$, both of which can be tuned over a wide range via laser intensity and static electric fields, respectively. The translation $X(t) = F(t)/(m\omega_0^2)$ of the Paul trap with respect to the optical lattice transports the ion crystal at adjustable speed, when the uniform electric force $F(t)$ is linearly ramped. The distribution of ion positions relative to the lattice can be tuned with nanometer precision via ω_0, allowing us to introduce a controlled structural mismatch between object (ion

Department of Physics, Massachusetts Institute of Technology, 77 Massachusetts Avenue, Cambridge, MA 02139, USA.
*These authors contributed equally to this work. **†Corresponding author. E-mail: vuletic@mit.edu**

crystal) and substrate (optical lattice). To remove the heat generated by friction, the ions are continuously laser cooled to temperatures much lower than the optical-lattice depth (*23*). We observe that the scattering of light by an ion is proportional to the ion's optical-lattice potential energy as a result of the lattice-assisted Raman cooling scheme (*23*, *28*). Thus, we can deduce the ion's position with subwavelength resolution during transport while its kinetic energy remains below its displacement-dependent potential energy—i.e., we can measure an ion's position before a slip and when it has cooled down again after a slip (*28*).

We first benchmark our nanofriction simulator against the PT model by transporting a single trapped ion in the corrugated potential V. Under intermediate corrugation, stick-slip results from the applied-force–induced switching between the two minima of a bistable potential (Fig. 1B). As the force $F(t)$ is linearly ramped up, the ion sticks in the initial site (no. 1), riding up the lattice potential and increasing in fluorescence (no. 2), until a critical maximum static friction force F_s is reached. At that point, the barrier vanishes and the initial minimum disappears, resulting in a fold catastrophe (*1*). The ion discontinuously slips from its initial site to the global minimum one site over (no. 3). The ion then dissipates the released energy ΔW via laser cooling, while localization in the lattice potential reduces its fluorescence again. The positions of fluorescence peaks in Fig. 2A thus correspond to the maximum static friction force F_s, when the ion slips. As the force ramp is reversed, hysteresis can be clearly observed in the shift $2F_s$ between the forward and reverse slips (Fig. 2A). The fluorescence increase leading up to each slip is converted to the ion's position to reconstruct the force-displacement curve enclosing the area $2\Delta W$ (Fig. 2B). We repeat the measurement at different values of the corrugation parameter $\eta = (\omega_L/\omega_0)^2$ and plot in Fig. 2C the maximum static friction force F_s versus η. For $\eta < 1$, friction vanishes, as there is no bistability, and the unique potential minimum is continuously translated by the applied force. For $1 < \eta < 4.60$, the potential is bistable and F_s increases with η (linearly in the large η limit). These results are in excellent agreement with the PT model (solid line in Fig. 2C). The regime with multiple minima $\eta > 4.60$

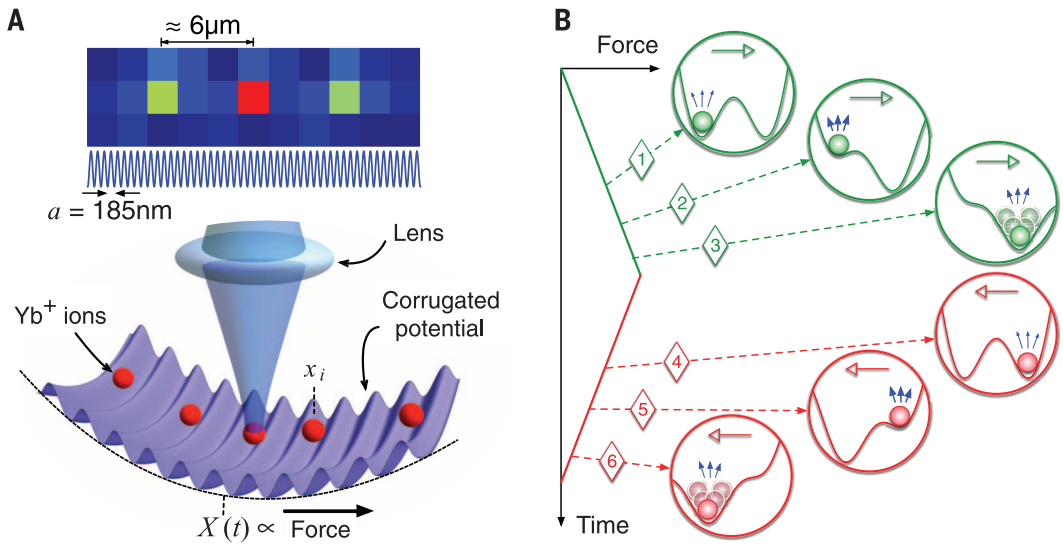

Fig. 1. Ion-crystal simulator of stick-slip friction. (**A**) Synthetic nanofriction interface between a Coulomb crystal of $^{174}Yb^+$ ions and an optical lattice, with single-ion-resolving microscope. The typical ion spacing is 6 μm, and the lattice period is a = 185 nm. In the bottom illustration of the corrugated potential, the lattice period and the corrugation are strongly exaggerated. (**B**) Stick-slip results from bistability, illustrated here for a single ion. We linearly ramp a shear force, causing the ion to jump between the minima, and we extract its position from its fluorescence, proportional to the lattice potential energy: (no. 1) ion initialized in the left site; (no. 2) the applied force pushes the ion up the lattice potential, eventually causing the slip; (no. 3) immediately after the slip, the ion is optically recooled and localizes to the right site; (no. 4), (no. 5), and (no. 6), the force ramp reverses and the ion sticks at the right site before slipping back to the left. Slips are identified by maxima in the ion's fluorescence.

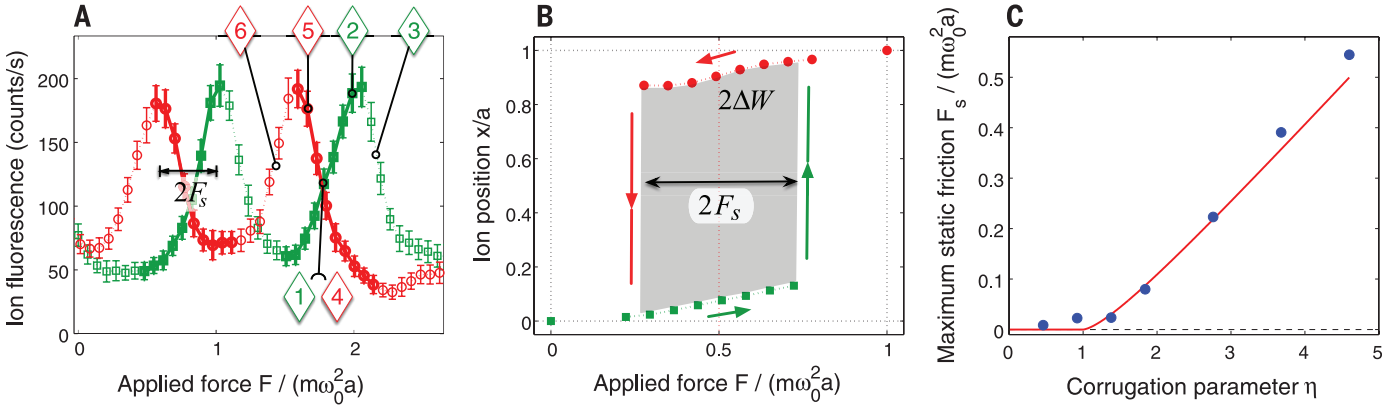

Fig. 2. Measured stick-slip hysteresis cycle of a single ion. (**A**) Fluorescence versus applied force during the forward transport (green squares) and reverse transport (red circles), showing hysteresis that is used to measure the maximum static friction force F_s. The stages of the stick-slip process (no. 1) to (no. 6) correspond to the illustrations in Fig. 1B. The bold data points indicate the ion's position before a slip, and only those data are used to reconstruct the force-displacement curve. (**B**) The force-displacement hysteresis loop encloses an area equal to twice the dissipated energy per slip ΔW. The unit $m\omega_0^2 a$ of the applied force corresponds to 2.8×10^{-19} N; here, $\omega_0 = 2\pi \times 364$ kHz. (**C**) The static friction force disappears for corrugations $\eta < 1$ and increases linearly with corrugation for $\eta > 1$, in excellent agreement with the Prandtl-Tomlinson model with no free parameters (red solid line). In (A), error bars indicate 1 SD, and for (B) and (C), statistical error bars are smaller than the symbols. The data in (A) and (B) were measured at $\eta = 2.8$.

results in more complicated multiple-slip patterns (*29*), sensitive to the recooling time constant, and is not explored here.

To study multiparticle models with a trapped ion crystal, we load a desired number of ions up to $N = 6$ and control their matching to the periodic optical-lattice potential via the electrostatic harmonic confinement ω_0. In the FK model, mismatch is manifested as incommensurability of the (infinite) object and substrate lattices.

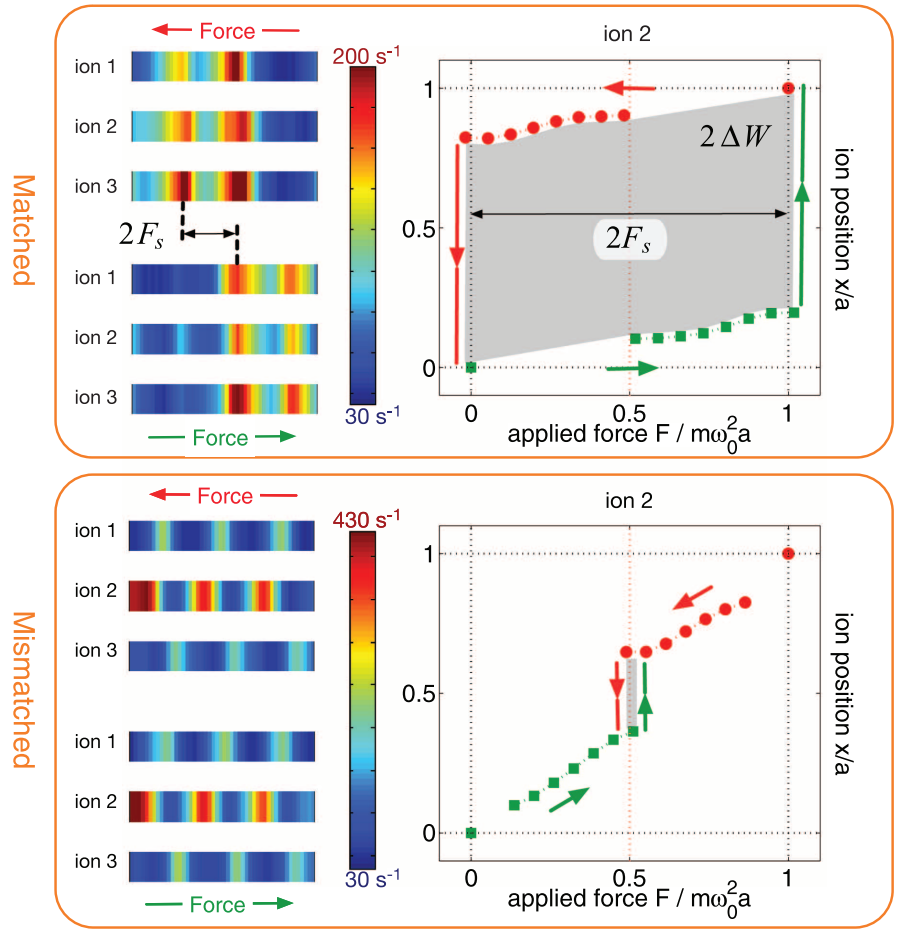

Fig. 3. Changing friction in a 3-ion crystal from maximal to nearly frictionless (superlubric) by structural mismatch. In the matched case (top), the ions stick and slip synchronously during transport (the observed photon detection rate for each ion, expressed in color, is maximum when the given ion slips over a potential barrier). The large hysteresis corresponds to large friction, shown here for the middle ion. In the mismatched case (bottom), the different ions slide over lattice barriers one at a time, and the friction and hysteresis nearly vanish.

Although our ion crystals are finite and inhomogeneous, we find that the essence of the FK model can be captured by introducing a matching parameter q that quantifies the alignment of the ions with equivalent points on the lattice when unperturbed by it. We define $q = \max_X \left[\frac{1}{N}\sum_i \sin(2\pi(x_{i0} - X)/a)\right]$, the maximum possible normalized averaged force of the optical lattice on the ions, when considering their lattice-free (unperturbed) equilibrium positions x_{i0} as the harmonic trap is displaced relative to the lattice. q is also related to the normalized potential barrier in the bistable energy landscape seen by the unperturbed ion crystal. By adjusting the Paul trap vibration frequency ω_0, we can continuously vary the q value (*28*) between $q = 1$, where each ion experiences an identical lattice force and the crystal behaves like a single particle (corresponding to the commensurate case in the FK model), and $q = 0$, where the lattice forces on the unperturbed crystal cancel out (analogous to an incommensurate arrangement).

For a selected matching parameter q, we drive the ion crystal across the lattice by linearly increasing the applied force and measure for each ion separately the stick-slip hysteresis, extracting F_s and ΔW. This is performed for crystal sizes from $N = 2$ to $N = 6$ ions at a value of η just below 4.60. As we switch from the matched case $q = 1$ to the mismatched case $q = 0$, we observe the friction change from maximal, corresponding to strong one-ion stick-slip friction for each ion, to nearly zero, corresponding to a superlubric regime, as shown in Fig. 3 for $N = 3$. Fluorescence of all three ions is plotted against the applied force in the forward and reverse directions, and the fluorescence peaks indicate the moment when each ion passes the barrier between two lattice sites. The data reveal that in the matched case, ions stick and slip together as a rigid body, with strong hysteresis between the forward and reverse transport, resulting in the maximal force-displacement hysteresis loop for each ion (middle ion shown), and maximal friction. By contrast, in the mismatched case, the ions move over the lattice in a staggered kink-like fashion, and each ion experiences almost no hysteresis or friction. Thus,

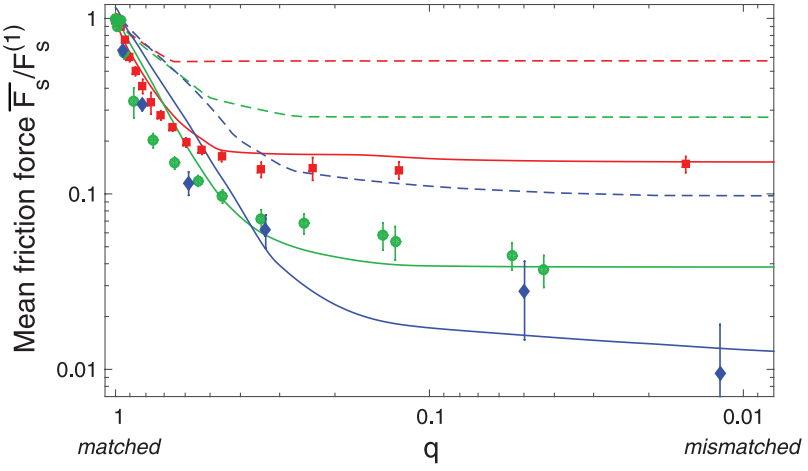

Fig. 4. The dependence of friction on object-substrate structural matching for different crystal sizes. Measured maximum static friction force F_s for $N = 2$, 3, and 6 ions (red squares, green circles, and blue diamonds, respectively), averaged over the ions and normalized to F_s as measured for a single trapped ion. Error bars represent 1 SD. Simulations for $N = 2$, 3, and 6 are shown for $T = 0$ (red, green, and blue dashed lines, respectively) and finite q-dependent temperature (red, green, and blue solid lines). Simulation parameters are chosen to match known experimental parameters: the measured temperature $k_BT(q = 1)/U \approx 0.05$ (corresponding to 48 μK); the optical-lattice depth $U/h = 20$ MHz (equivalent to $\eta = 4.6$); the driving velocity $v = 0.4$mm/s; and the recooling rate constant from laser cooling $r = 2\pi \times 3$ kHz. Only the $q = 0$ temperature is fitted, yielding $k_BT(q = 0)/U = 0.15$ (corresponding to 144 μK) for all the values of N shown [see (*28*)].

the structural suppression of friction is accompanied by a transition in the nature of transport from a simultaneous slipping regime reducible to an effective single-particle PT model, to a kink propagation regime characteristic of the infinite FK model.

In Fig. 4, we plot the measured maximum static friction force $\overline{F_s}$, averaged over the ions in the crystal, versus the matching q. (The dissipated energy $\overline{\Delta W}$ follows the same q dependence). As q is lowered from 1, the friction drops quickly, then slowly approaches a much reduced value at $q = 0$, which decreases with increasing crystal size. Notably, at $q = 0$ (mismatched limit) there is an almost 10-fold reduction in friction already for $N = 2$ ions, and a 100-fold reduction for $N = 6$ ions. Numerical simulations of this behavior at zero temperature (dashed lines in Fig. 4) show qualitative agreement but fail to account for the finite temperature of the ions in the experiment. For lower q values, the effective barrier separating two potential minima is reduced, and the friction becomes more sensitive to temperature (*28*). To take temperature-induced friction reduction (thermolubricity) (*1*) into account, we perform full dynamics simulations accounting for the finite crystal temperature (*28*) and find good agreement with the experiment (solid lines in Fig. 4). These simulations indicate that in the limit of low q, thermolubricity and superlubricity (mismatch-induced lubricity) reduce the observed friction by similar factors in our data.

Our results indicate that it may be possible to engineer nanofriction by structural control in finite-size systems. Intriguing future possibilities include the coupling to internal states of the ions (*30*) for the study of spin-dependent transport and friction (*22*) and the regime of weak periodic potentials, where quantum-mechanical tunneling may lead to new quantum phases (*19*, *22*).

REFERENCES AND NOTES

1. A. Vanossi, N. Manini, M. Urbakh, S. Zapperi, E. Tosatti, *Rev. Mod. Phys.* **85**, 529–552 (2013).
2. M. Urbakh, J. Klafter, D. Gourdon, J. Israelachvili, *Nature* **430**, 525–528 (2004).
3. V. Bormuth, V. Varga, J. Howard, E. Schäffer, *Science* **325**, 870–873 (2009).
4. C. H. Scholz, *Nature* **391**, 37–42 (1998).
5. K. Shinjo, M. Hirano, *Surf. Sci.* **283**, 473–478 (1993).
6. L. Prandtl, *Z. Angew. Math. Mech.* **8**, 85–106 (1928).
7. G. A. Tomlinson, *Philos. Mag.* **7**, 905–939 (1929).
8. O. M. Braun, Y. S. Kivshar, *The Frenkel-Kontorova Model: Concepts, Methods, and Applications* (Springer, New York, 2004).
9. Y. I. Frenkel, T. A. Kontorova, *Zh. Eksp. Teor. Fiz.* **8**, 1340 (1938).
10. S. Aubry, *Physica D* **7**, 240–258 (1983).
11. G. Binnig, C. F. Quate, C. Gerber, *Phys. Rev. Lett.* **56**, 930–933 (1986).
12. C. M. Mate, G. M. McClelland, R. Erlandsson, S. Chiang, *Phys. Rev. Lett.* **59**, 1942–1945 (1987).
13. R. W. Carpick, M. Salmeron, *Chem. Rev.* **97**, 1163–1194 (1997).
14. I. Szlufarska, M. Chandross, R. W. Carpick, *J. Phys. D* **41**, 123001 (2008).
15. A. Socoliuc, R. Bennewitz, E. Gnecco, E. Meyer, *Phys. Rev. Lett.* **92**, 134301 (2004).
16. M. Dienwiebel *et al.*, *Phys. Rev. Lett.* **92**, 126101 (2004).
17. M. Hirano, K. Shinjo, R. Kaneko, Y. Murata, *Phys. Rev. Lett.* **78**, 1448–1451 (1997).
18. T. Bohlein, J. Mikhael, C. Bechinger, *Nat. Mater.* **11**, 126–130 (2011).
19. I. García-Mata, O. V. Zhirov, D. L. Shepelyansky, *Eur. Phys. J. D* **41**, 325–330 (2007).
20. A. Benassi, A. Vanossi, E. Tosatti, *Nat. Commun.* **2**, 236 (2011).
21. D. Mandelli, A. Vanossi, E. Tosatti, *Phys. Rev. B* **87**, 195418 (2013).
22. T. Pruttivarasin, M. Ramm, I. Talukdar, A. Kreuter, H. Häffner, *New J. Phys.* **13**, 075012 (2011).
23. L. Karpa, A. Bylinskii, D. Gangloff, M. Cetina, V. Vuletić, *Phys. Rev. Lett.* **111**, 163002 (2013).
24. R. B. Linnet, I. D. Leroux, M. Marciante, A. Dantan, M. Drewsen, *Phys. Rev. Lett.* **109**, 233005 (2012).
25. M. Enderlein, T. Huber, C. Schneider, T. Schaetz, *Phys. Rev. Lett.* **109**, 233004 (2012).
26. D. Leibfried, R. Blatt, C. Monroe, D. Wineland, *Rev. Mod. Phys.* **75**, 281–324 (2003).
27. M. Cetina *et al.*, *New J. Phys.* **15**, 053001 (2013).
28. Materials and methods are available as supplementary material on *Science* Online.
29. S. N. Medyanik, W. K. Liu, I.-H. Sung, R. W. Carpick, *Phys. Rev. Lett.* **97**, 136106 (2006).
30. J. Mizrahi *et al.*, *Phys. Rev. Lett.* **110**, 203001 (2013).

ACKNOWLEDGMENTS

We thank W. Jhe and E. Demler for stimulating discussions and W. Jhe also for critical reading of the manuscript. This work was supported by the NSF-funded Center for Ultracold Atoms (grant PHY-0551153) and Canada's *Natural Sciences and Engineering Research Council* Postgraduate Scholarship program. All data presented here is in the supplementary materials.

SUPPLEMENTARY MATERIALS

www.sciencemag.org/content/348/6239/1115/suppl/DC1
Materials and Methods
Fig. S1
Database S1
Reference (*31*)

18 September 2014; accepted 1 May 2015
10.1126/science.1261422

FRICTION

Macroscale superlubricity enabled by graphene nanoscroll formation

Diana Berman,[1] Sanket A. Deshmukh,[1] Subramanian K. R. S. Sankaranarayanan,[1] Ali Erdemir,[2] Anirudha V. Sumant[1]*

Friction and wear remain as the primary modes of mechanical energy dissipation in moving mechanical assemblies; thus, it is desirable to minimize friction in a number of applications. We demonstrate that superlubricity can be realized at engineering scale when graphene is used in combination with nanodiamond particles and diamondlike carbon (DLC). Macroscopic superlubricity originates because graphene patches at a sliding interface wrap around nanodiamonds to form nanoscrolls with reduced contact area that slide against the DLC surface, achieving an incommensurate contact and substantially reduced coefficient of friction (~0.004). Atomistic simulations elucidate the overall mechanism and mesoscopic link bridging the nanoscale mechanics and macroscopic experimental observations.

Macroscopic friction and wear remain the primary modes of mechanical energy dissipation in moving mechanical assemblies such as pumps, compressors, and turbines, leading to unwanted material loss and wasted energy. It is estimated that nearly one third of the fuel used in automobiles is spent to overcome friction, while wear limits mechanical component life. Even a modest 20% reduction in friction can substantially affect cost economics in terms of energy savings and environmental benefits (*1*). In that context, superlubricity is desirable for various applications and therefore is an active area of research. To date, superlubricity has been primarily realized in a limited number of experiments involving atomically smooth and perfectly crystalline materials (*2*–*5*) and supported by theoretical studies (*6*, *7*). Superlubricity has been demonstrated for highly oriented pyrolytic graphite (HOPG) surfaces (*8*), as well as for multiwalled carbon nanotubes (MWCNTs), when the conditions for incommensurate contacts are met in a dry environment (*9*). Because these conditions are due to the incommensurability of lattice planes sliding against each other, they are referred to as structural lubricity and restricted to material interactions at the nanoscale. At the macroscale, this structural effect (hence, superlubricity) is lost because of the structural imperfections and disorder caused by many defects and deformations.

Low friction has recently been observed in centimeter-long double-walled carbon nanotubes with perfect atomic structures and long periodicity (*10*). Ultralow friction in disordered solid interfaces, such as self-mated DLC films (*11*–*14*) and in fullerenelike nanoparticles such as molybdenum disulfide (MoS_2) (*15*), has been observed under specific environmental and sliding conditions. However, the exact superlubricity mechanism in the above cases is still debatable and is not realized for industrial applications. In recent studies at the nano- and macroscale, graphene has shown a potential to substantially lower friction (*16*–*18*) and wear (*19*–*21*) under specific

[1]Center for Nanoscale Materials, 9700 South Cass Avenue, Argonne National Laboratory, Argonne, IL 60439, USA.
[2]Energy Systems Division, 9700 South Cass Avenue, Argonne National Laboratory, Argonne, IL 60439, USA.
***Corresponding author. E-mail: sumant@anl.gov**

Tuning friction atom-by-atom in an ion-crystal simulator

Alexei Bylinskii *et al.*

Science **348**, 1115 (2015);
DOI: 10.1126/science.1261422